

FORMATION AND STRUCTURE OF IRON-IMPURITY COMPLEXES IN SILICON

C.A.J. Ammerlaan

Natuurkundig Laboratorium, Universiteit van Amsterdam
Valckenierstraat 65, NL-1018 XE Amsterdam, The Netherlands

ABSTRACT

Precipitation of iron impurity atoms in silicon proceeds in its early stages via the formation of iron-iron pairs, iron-impurity pairs and complexes consisting of a few atoms. The structure of such aggregates can be investigated by magnetic resonance. Angular variation of the spectra reveals the symmetry of the centres. An analysis of the g-values of the resonances gives the number of iron atoms in the centres and their charge state. Independently, the number of iron atoms is obtained from the hyperfine structure in the spectra using the mass-57 magnetic isotope of iron. The results show the atomic details of the heterogeneous nucleation of the precipitation process.

1. INTRODUCTION

Iron is a common impurity in silicon crystals. Even when the basic material was very pure, the impurity is easily introduced from contamination of wafer surfaces by processing treatments such as cutting and covering with etch resists. During thermal anneal surface impurity atoms rapidly penetrate the bulk of the crystals. Precipitation of impurities occurs when the impurity solubility concentration at high process temperatures exceeds that of lower, typical room, temperature, when the mobility at room temperature of impurity atoms is still sufficiently high, and when nucleation sites are provided [1]. For iron in silicon these three conditions are met and consequently precipitation effects will occur. In this paper illustrations will be given of the earliest steps in this process. The next section of the paper will discuss in some detail the application of electron paramagnetic resonance (EPR) to identify the chemical nature of impurity constituents in the centres, their charge state, and the constraints on the symmetry of the geometrical arrangements of atoms and other structural units in the centres. This will lead to quite a detailed understanding of the structure of iron-iron pairs, iron-impurity pairs and other small iron-related aggregates that can be generated in the process of heterogeneous nucleation.

Table I. Iron and iron-related centres in silicon: parameters in spin-Hamiltonians of electron paramagnetic resonance spectra analysed with low value of effective spin S .

Spectrum	Model	Symmetry	Spin S	Principal g -values			Reference
				g_1	g_2	g_3	
Fe ⁰	Fe _i ⁰	Cubic	1	2.0699	2.0699	2.0699	[2]
Fe ⁺	Fe _i ⁺	Cubic	1/2	3.524	3.524	3.524	[3]
FeB	(Fe _i B _S) ⁰ -pair	Trigonal	1/2	2.0676	4.0904	4.0904	[4]
NL27	(Fe _i Al _S) ⁰ -pair	Trigonal	1/2	6.389	1.138	1.138	[5]
NL28	(Fe _i Al _S) ⁰ -pair	Orthorhombic-I	1/2	5.885	1.236	1.612	[5]
FeAl(3)	(Fe _i Al _S) ⁰ -pair	Orthorhombic-I	1/2	5.36	2.51	1.73	[6]
FeGa(1)	(Fe _i Ga _S) ⁰ -pair	Trigonal	1/2	5.089	2.530	2.530	[3]
FeGa(2)	(Fe _i Ga _S) ⁰ -pair	Orthorhombic-I	1/2	6.19	0.59	0.69	[6]
FeGa(3)	(Fe _j Ga _S) ⁰ -pair	Orthorhombic-I	1/2	2.02	3.37	4.65	[6]
FeIn	(Fe _i In _S) ⁰ -pair	Orthorhombic-I	1/2	2.07	3.78	4.40	[7]
FeS(I)	Fe _i S _S -pair	Monoclinic-I	1/2	2.126	2.046	2.010	[8]
FeS(II)	Fe _i S _S -pair	Monoclinic-I	1/2	2.015	2.962	1.938	[8]
FeS(III)	Fe _i S _S -pair	Monoclinic-I	1/2	2.042	2.503	1.991	[8]
FeS(IV)	Fe _i S _S -pair	Monoclinic-I	1/2	1.9564	2.6910	1.9390	[9]
PdFe	Pd _S Fe _i -pair	Trigonal	1/2	2.0407	2.0887	2.0887	[10]
Pt(II)	Pt _S Fe _i -pair	Trigonal	1/2	2.0124	2.1264	2.1264	[10]
A23	Au _S Fe _i -pair	Trigonal	1/2	2.0993	2.1165	2.1165	[11]
A25	(FePI/V) ⁺ -complex	Monoclinic-I	1/2	2.093	2.067	2.153	[12]
A26	(FePI/V) ⁰ -complex	Monoclinic-I	1/2	2.131	2.056	2.138	[12]
A27	FeBV/I-complex	Monoclinic-I	1/2	4.78	1.96	3.24	[12]
A28	FeOV-complex	Monoclinic-I	1/2	4.20	2.15	4.10	[12]
NL19	Fe _S ⁺	Trigonal	3/2	2.1163	2.0935	2.0935	[13]
NL20	(Fe _i Fe _i V) ⁻ -complex	Trigonal	1/2	2.059	6.235	6.235	[13]
NL21	Fe _i Fe _i V ₂ -complex	Monoclinic-I	1/2	4.90	1.961	7.38	[13]
NL22	(Fe _i) ₄ -complex	Trigonal	4	2.075	2.068	2.068	[13]
NL23	Fe _i -complex	Triclinic	1/2	5.489	2.809	1.768	[13]
NL24	(Fe _i Fe _i) ⁺ -pair	Monoclinic-I	1/2	1.15	2.06	9.44	[14]
FeFe(2)	Fe _i Fe _i -pair	Monoclinic-I	1/2	3.90	3.50	5.07	[15]
NL25	Fe _i Fe _i -complex	Orthorhombic-II	5/2	2.51	1.47	0.57	[13]
FeFeB(1)	Fe _i Fe _i B-complex	Monoclinic-I	1/2	1.472	2.895	8.899	[16]
FeFeB(2)	Fe _i Fe _i B-complex	Monoclinic-I	1/2	3.05	2.96	5.46	[15]
FeFeB(3)	Fe _i Fe _i B-complex	Orthorhombic-I	1/2	1.811	4.184	7.902	[16]
FeFeB(4)	Fe _i Fe _i B-complex	Orthorhombic-I	1/2	5.80	1.94	1.73	[15]

2. MAGNETIC RESONANCE

2.1. SYMMETRY

The silicon crystal structure, which is identical to diamond, is characterized by its crystallographic space group. Viewed from a given site the crystal will be invariant under point group operations, specific for the site. For instance, around the substitutional site a $\bar{4}3m$ point group symmetry will exist. The inclusion of atomic or small defects in the host crystal may destroy such symmetry operations. In the most severe case a centre has no symmetry operations at all by itself. Such a centre, of intrinsic triclinic symmetry, when embedded in silicon will annul all the crystal symmetry operations. On the other extreme, a single atom, having cubic symmetry, when occupying a substitutional lattice site will leave all crystal symmetry operations intact. In between these extreme cases situations exist where the centre cancels part of the crystal symmetries, while leaving others in existence. As a result analysis shows that eight cases can be distinguished to all of which different well-defined groups of symmetry operations belong. These are: cubic, trigonal, tetragonal, orthorhombic-I, orthorhombic-II, monoclinic-I, monoclinic-II, and triclinic, roughly in order of decreasing symmetry.

Impurities with identical structure can still be embedded in the silicon crystal in different orientations. The lower the symmetry of the centre itself, the higher the number of orientations that are distinguishably different. For instance, a triclinic centre will have 24 different orientations. Properties which are sensitive to angular coordinates will yield different values for each of the 24 orientations. As an example in magnetic resonance each of the orientations will in general have a different value of the magnetic field at resonance. This directly establishes an unambiguous relation between the number of observable resonances and the symmetry of the centre, in terms of the 8 systems mentioned. The different orientations and positions of a centre can be transformed into each other by the space group of the crystal. Required by this symmetry, certain relations will exist between the components of the tensors describing the anisotropic properties. This leads to orientational degeneracy, which implies that for high-symmetry crystallographic directions of the measuring fields several orientations give coinciding results. In such way, all 8 symmetry cases are characterized by typical patterns of angular dependence. Figure 1 gives illustrations of angular variation as observed in electron paramagnetic resonance for some iron-related centres. The magnetic field is rotated in the (011) crystal plane from the [100] to the [011] direction. The examples include the spectrum NL23 which reveals the lowest possible triclinic symmetry for the paramagnetic centre, and consequently the maximum number of resonances. By inspection of the figures 1(a) to 1(d) one can also conclude that different symmetries are characterized by patterns with different numbers of resonances and essentially different schemes of coincidences in the directions [100], [111] and [011]. A summary of crystallographic symmetries as found for iron and iron-related centres in silicon is given in Table I. Obviously, atomic models to account for the centres must be consistent with these experimentally established symmetries.

2.2. g-VALUES

2.2.1. SPIN $S=1/2$

Table I also shows the principal values of the g-tensor giving the Zeeman splitting induced by a magnetic field. Results are based on an analysis of the observed resonance field values with a lowest possible value of the effective spin S . In most, though not in all, cases an analysis with $S = 1/2$ is possible

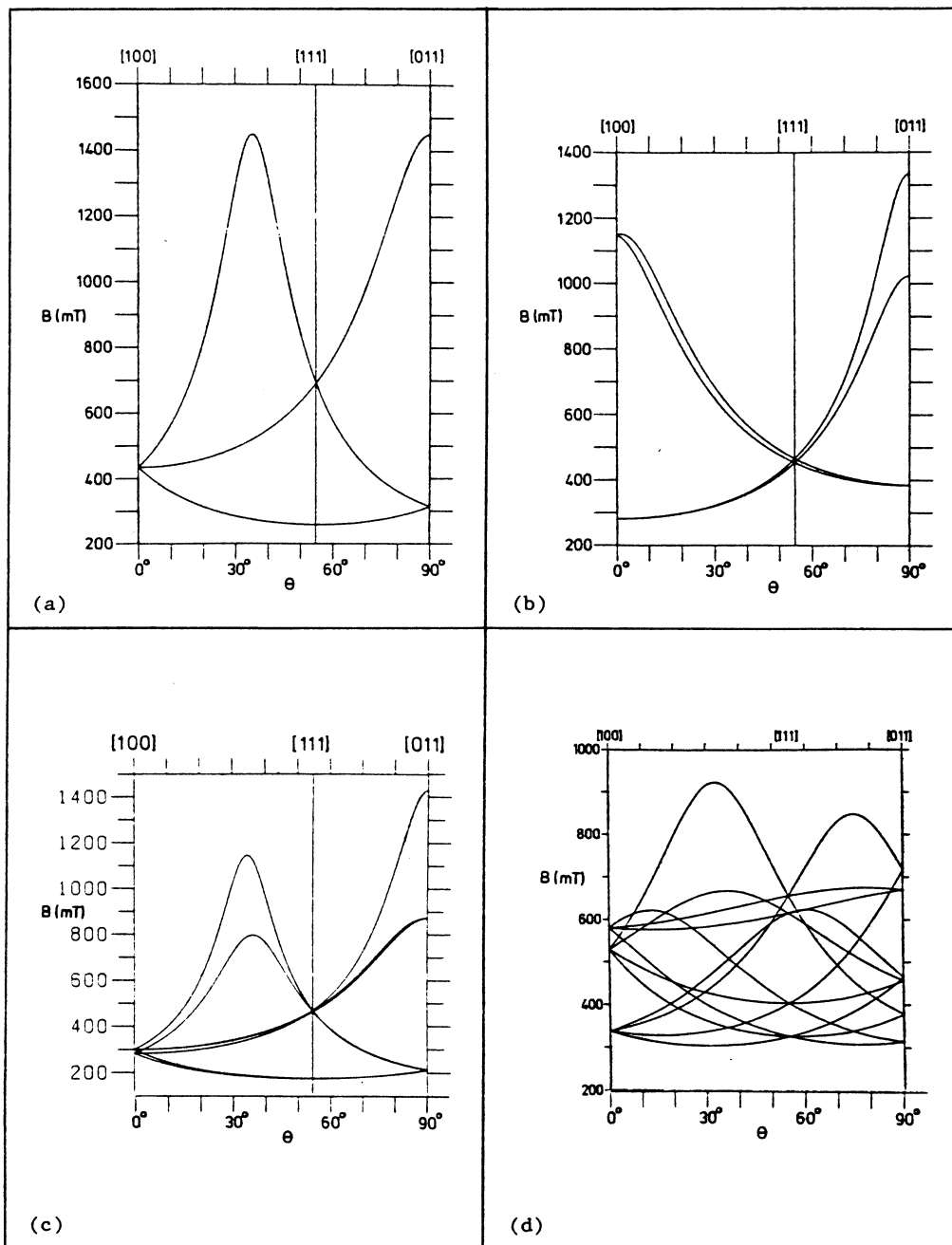


Figure 1. Angular dependence of the magnetic field at resonance, for rotation of \vec{B} in the (011) plane, for a microwave frequency 23 GHz, for: (a) spectrum NL27 revealing trigonal symmetry, (b) spectrum NL28 of an orthorhombic-I centre, (c) spectrum NL24 of a monoclinic-I centre, and (d) spectrum NL23 of a triclinic centre.

to match the experimental data. The simple spin-Hamiltonian to describe the fine structure of the spectrum is

$$\mathcal{H} = +\mu_B \vec{B} \cdot \vec{g} \cdot \vec{S}. \quad (1)$$

In case of cubic centres the g-tensor reduces to one scalar numerical value: $g_1 = g_2 = g_3 = g$. For trigonal centres the axial symmetry leads to $g_1 = g_{\parallel}$ and $g_2 = g_3 = g_{\perp}$. For monoclinic-I centres the orientation angle θ , not given in table I, is to be found in the original literature. For the centres for which results for $S = 1/2$ are presented in table I a satisfactory match between the experiment and the transition energies from equation (1) is obtained. The analysis has the advantage of giving unique results for the g-tensor elements. However, table I shows that in many cases g-values differing substantially from $g = 2$ are obtained. For centres of low symmetry, which all centres except Fe_1^+ actually have, no significant orbital contributions are expected. For spin-only magnetism $g \neq 2$ may be considered as unphysical. This indicates that the spin doublet in which the magnetic resonance is observed is not well separated in energy from other levels in a multiplet with more than two levels. In other words, an analysis with effective spin higher than $1/2$ is more appropriate.

2.2.2. SPIN $S=3/2$

In case of higher effective spin several electrons, or holes, must be present in the centre. The interaction between them is represented by additional terms in the spin-Hamiltonian. For spin $S = 3/2$ the Hamiltonian is augmented by:

$$\mathcal{H} = +D(S_z^2 - 5/4) + E(S_x^2 - S_y^2). \quad (2)$$

In this expression the first term represents an axial interaction taken along the z-axis. The last term gives an orthorhombic contribution. Effective spin $S = 3/2$ will describe the states in a quartet. Basis states are specified as $|m_S\rangle = |-3/2\rangle, |-1/2\rangle, |+1/2\rangle$ and $|+3/2\rangle$. Operating with the Hamiltonian of equation (2) on these states will produce a matrix with elements $\langle m_S | \mathcal{H} | m_S \rangle$ from which eigenvalues and eigenstates are derived. Due to the remaining Kramers degeneracy two doublets of levels are obtained. The energies $\epsilon_{+/-}$ are given by

$$\epsilon_{+/-} = \pm(D^2 + 3E^2)^{1/2}. \quad (3)$$

The corresponding eigenstates are

$$|\Phi_i\rangle = +\cos\phi_i | +3/2\rangle + \sin\phi_i | -1/2\rangle, \quad (4a)$$

$$|\Phi_i^*\rangle = +\cos\phi_i | -3/2\rangle + \sin\phi_i | +1/2\rangle, \quad (4b)$$

with

$$\text{tg}\phi_i = (-D + \epsilon_i)/E/3. \quad (4c)$$

On these states the Zeeman effect, given by equation (1), can be applied as a perturbation. The crystal field terms will determine the major effect on the anisotropy. For simplicity, the Zeeman interaction can therefore be taken as isotropic with g-value equal to 2, or at least very close to this value. Application of the magnetic field will split the levels of the doublets. Transitions between the levels, the electron paramagnetic resonance, will be observable in the ground state doublet. At high enough temperatures the higher

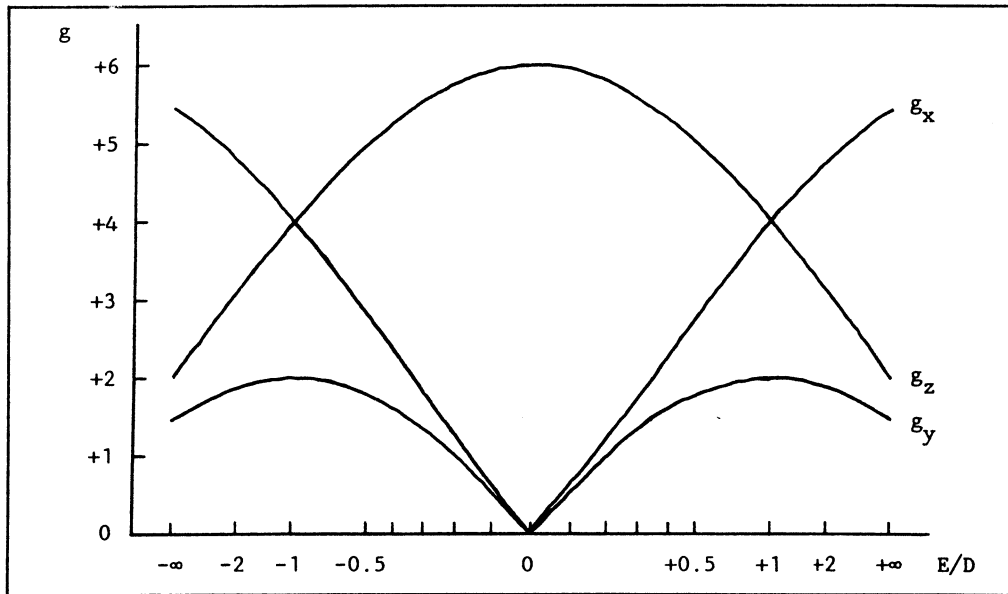


Figure 2. Principal values g_x , g_y and g_z of the g -tensor as a function of the ratio E/D of orthorhombic to trigonal crystal field, for spin $S = 3/2$.

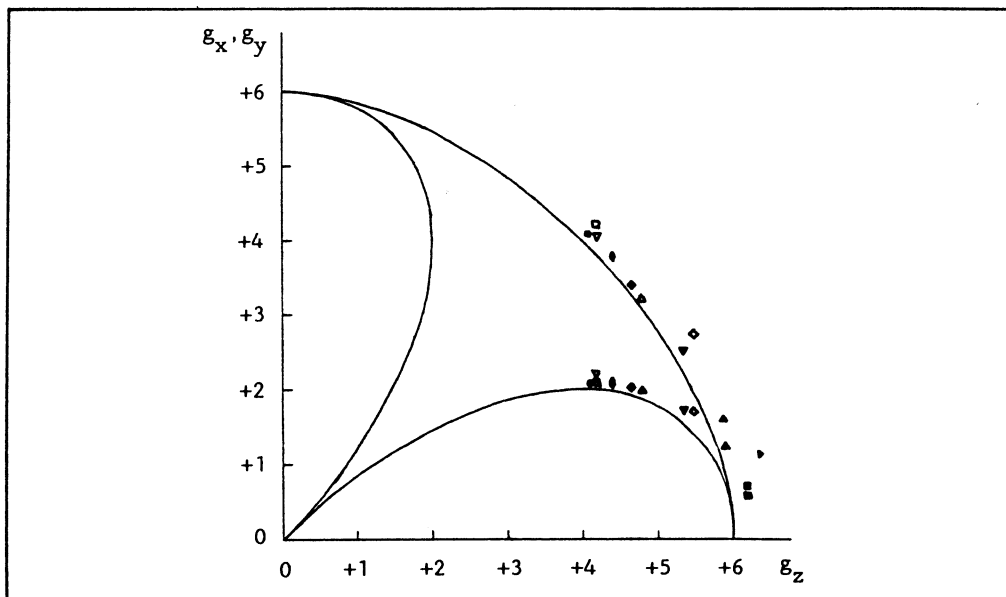


Figure 3. Relation between the principal values g_x , g_y and g_z of the g -tensor for spin $S = 3/2$ and experimental data points for several iron-related centres: FeB (●), NL27 (◀), NL28 (▲), FeAl(3) (▼), FeGa(2) (■), FeGa(3) (◆), FeIn (◊), A27 (△), A28 (▽), NL19 (◻) and NL23 (◊).

lying doublet may be populated as well and an additional resonance is then observable. The g -values of the Zeeman splitting are given by:

$$g_x = +2 \pm (-2D + 6E)/(D^2 + 3E^2)^{1/2}, \quad (5a)$$

$$g_y = -2 \pm (+2D + 6E)/(D^2 + 3E^2)^{1/2}, \quad (5b)$$

$$g_z = +2 \pm 4D/(D^2 + 3E^2)^{1/2}. \quad (5c)$$

In figure 2 plots are given of these g -values as a function of the dimensionless parameter E/D , which is the ratio of orthorhombic to axial crystal field. By elimination of E/D a relation can be obtained between the g -values g_x , g_y and g_z . The result is given in figure 3. A plot as figure 3 is also suitable for a direct representation of experimental data of principal g -values. Included in the figure are the results as given in Table I for the centres FeB, NL27, NL28, FeAl(3), FeGa(2), FeGa(3), FeIn, A27, A28, NL19, and NL23. From the good correspondence it is concluded that this kind of analysis is adequate. Compared to the previous analysis with $S = 1/2$ the present analysis has the advantages that: (1) a better fit of the angular dependence in the experiment and the theory is obtained, (2) a physically justifiable g -value $g = 2$ has been used, (3) information on the crystal fields is obtained by determination of E/D , and (4) the real spin corresponding to the number of coupled spins is obtained. Apparently the spin $S = 3/2$ is related to three electron spins coupled in parallel. For iron this actually is better described by three holes in the 3d shell leading to electronic configuration $(3d)^7$. The corresponding atomic configuration is one positively charged interstitial iron atom: Fe_i^+ .

2.2.3. SPIN $S=5/2$

In just the same way as for $S = 3/2$ the case of effective spin $S = 5/2$ can be treated. Basis states spanning the sextet are taken as $|m_S\rangle = |-5/2\rangle, |-3/2\rangle, |-1/2\rangle, |+1/2\rangle, |+3/2\rangle$ and $|+5/2\rangle$. Interaction between the electron spins is accounted for by the Hamiltonian

$$\mathcal{H} = +D(S_z^2 - 35/12) + E(S_x^2 - S_y^2). \quad (6)$$

Energies and eigenstates again follow from diagonalization of the matrix $\langle m_S | \mathcal{H} | m_S \rangle$. In this case the solution of the cubic equation yields the energies of the three doublets. The wave functions are expressed by

$$|\Phi_i\rangle = a_i |+5/2\rangle + b_i |+1/2\rangle + c_i |-3/2\rangle, \quad (7a)$$

$$|\Phi_i^*\rangle = a_i |-5/2\rangle + b_i |-1/2\rangle + c_i |+3/2\rangle, \quad (7b)$$

with the coefficients a_i , b_i and c_i found from the eigenvalue equation. In terms of the wave function coefficients the g -values are given by

$$g_x = +6b_i^2 + 4/5a_i c_i + 8/2b_i c_i, \quad (8a)$$

$$g_y = +6b_i^2 + 4/5a_i c_i - 8/2b_i c_i, \quad (8b)$$

$$g_z = +10a_i^2 + 2b_i^2 - 6c_i^2. \quad (8c)$$

Figure 4 shows g_x , g_y and g_z as a function of E/D . The relation between the principal g -values is illustrated by figure 5. Data from the experimental determinations, as given in table I, are plotted in figure 5 for the centres

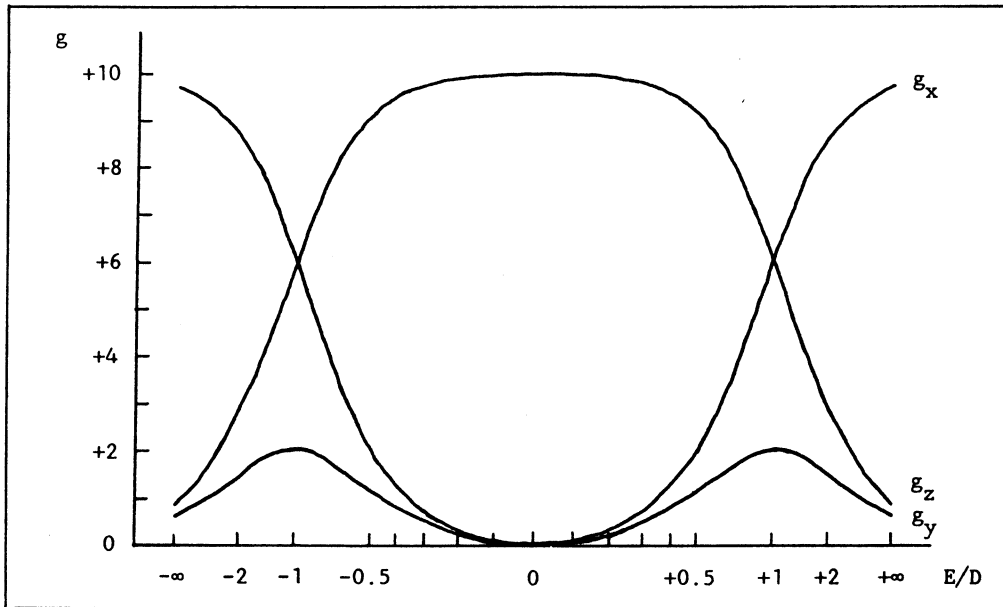


Figure 4. Principal values g_x , g_y and g_z of the g-tensor as a function of the ratio E/D of orthorhombic to trigonal crystal field, for spin $S = 5/2$.

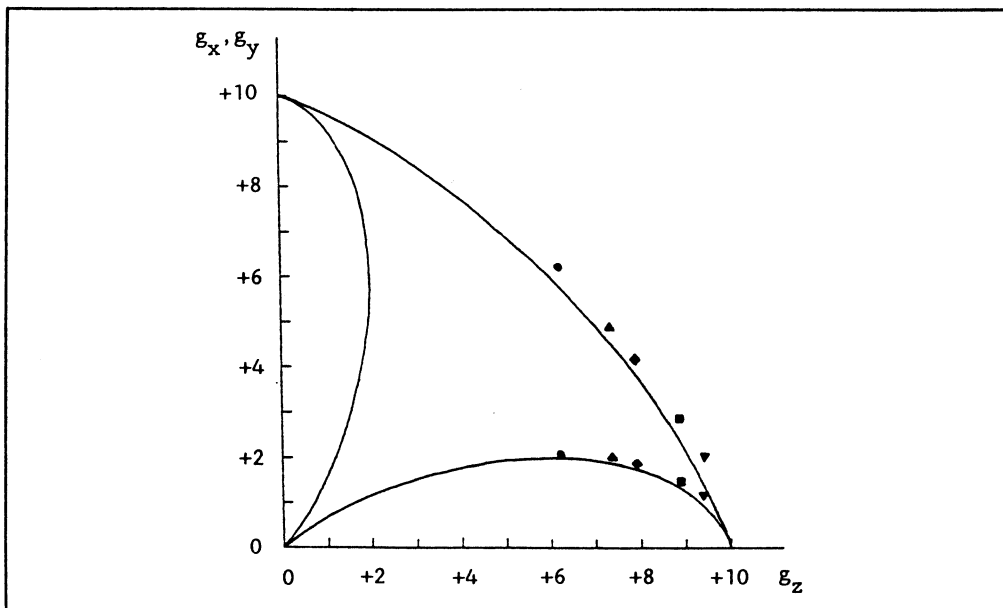


Figure 5. Relation between the principal values g_x , g_y and g_z of the g-tensor for spin $S = 5/2$ and experimental data points for several iron-related centres: NL20 (●), NL21 (▲), NL24 (▼), FeFeB(1) (■) and FeFeB(3) (◆).

NL20, NL21, NL24, FeFeB(1) and FeFeB(3). From the good agreement the conclusion is drawn that effective spin $S = 5/2$ is the physically correct value for the spin of these centres. This spin corresponds to 5 electrons of which the spin is parallel as a result of Hund's rule or ferromagnetic exchange coupling. Such an electronic configuration $[(3d)^8(3d)^8]_h$ arises from a positive pair of interstitial iron atoms: $(Fe_i Fe_i)^+$.

2.3. HYPERFINE STRUCTURE

An unambiguous way of demonstrating the presence of an impurity is the observation of hyperfine interaction due to a magnetic isotope of the element. For iron the isotope with mass 57 has nuclear spin $I = 1/2$, but only a natural abundance of 2.2%. Therefore, in order to obtain hyperfine split-off lines with sufficient intensity the use of enriched material is mandatory. In the spin-Hamiltonian the hyperfine interaction is accounted for by a term

$$\mathcal{H} = \mathcal{A} \cdot \mathcal{S} \cdot \mathcal{I} \quad (9)$$

where the tensor \mathcal{A} gives the strength of the interaction between electron spin S and one nuclear spin I . A solution valid to first order gives energy changes $A_{eff} m_S m_I$ of the energy levels and a change $A_{eff} m_I$ of the EPR transition energy. The EPR spectrum will consequently be split into two components corresponding to $m_I = +1/2$ and $-1/2$, respectively. For an isotopic fraction α each of the hyperfine lines will have intensity $\alpha/2$ compared to intensity $1-\alpha$ of the central line from the non-magnetic isotopes. Such splitting is illustrated in the figures 6(a) and 6(b). In both cases also hyperfine interaction is resolved with a second magnetic impurity isotope with 100% natural abundance. In the NL28 spectrum corresponding to the FeAl-pair the aluminium nucleus, ^{27}Al with $I = 5/2$, dominates the structure (figure 6(a), top). Similarly for spectrum A23 of the AuFe-pair the major splitting is due to the ^{197}Au nucleus with $I = 3/2$, as shown in figure 6(b), top. The iron nucleus manifests itself as a smaller additional splitting of resonance lines. Obviously, this hyperfine structure reveals much of the details of the composition of the centres. When more than one iron atom forms part of the centre the hyperfine structure becomes more involved. For two atoms on equivalent sites, with equal hyperfine interaction strength, one expects a splitting into five equidistant components. For isotopic concentration α the intensities are predicted to scale as $\alpha^2/4 : \alpha(1-\alpha) : (1-\alpha)^2 + \alpha^2/2 : \alpha(1-\alpha) : \alpha^2/4$. For an enrichment $\alpha = 90\%$ the calculated ratios are 20 : 9 : 42 : 9 : 20. Such ratios are found experimentally for several of the centres, as can be verified for NL21 and NL24 in the figures 6(c) and 6(d). This provides the experimental demonstration of the presence of two iron atoms.

3. CONCLUSION

In table I the magnetic resonance spectra which have been demonstrated to correspond to iron-related centres in silicon are listed. A few of these spectra may arise from excited state doublets for which another spectrum is related to the ground state. In spite of this possible ambiguity, a formidable number of small iron-related centres has been identified. The hyperfine structure, either due to naturally present isotopes or as a result of intentional doping, provides clear evidence on the presence of impurities in the centres. An analysis of g -values gives confirmation on the number of iron atoms in the centre and determines the number of electrons present, hence the charge state of the centre. Finally, the interaction tensors reveal the symmetry of the geometrical arrangement in which the constituents of the centre can

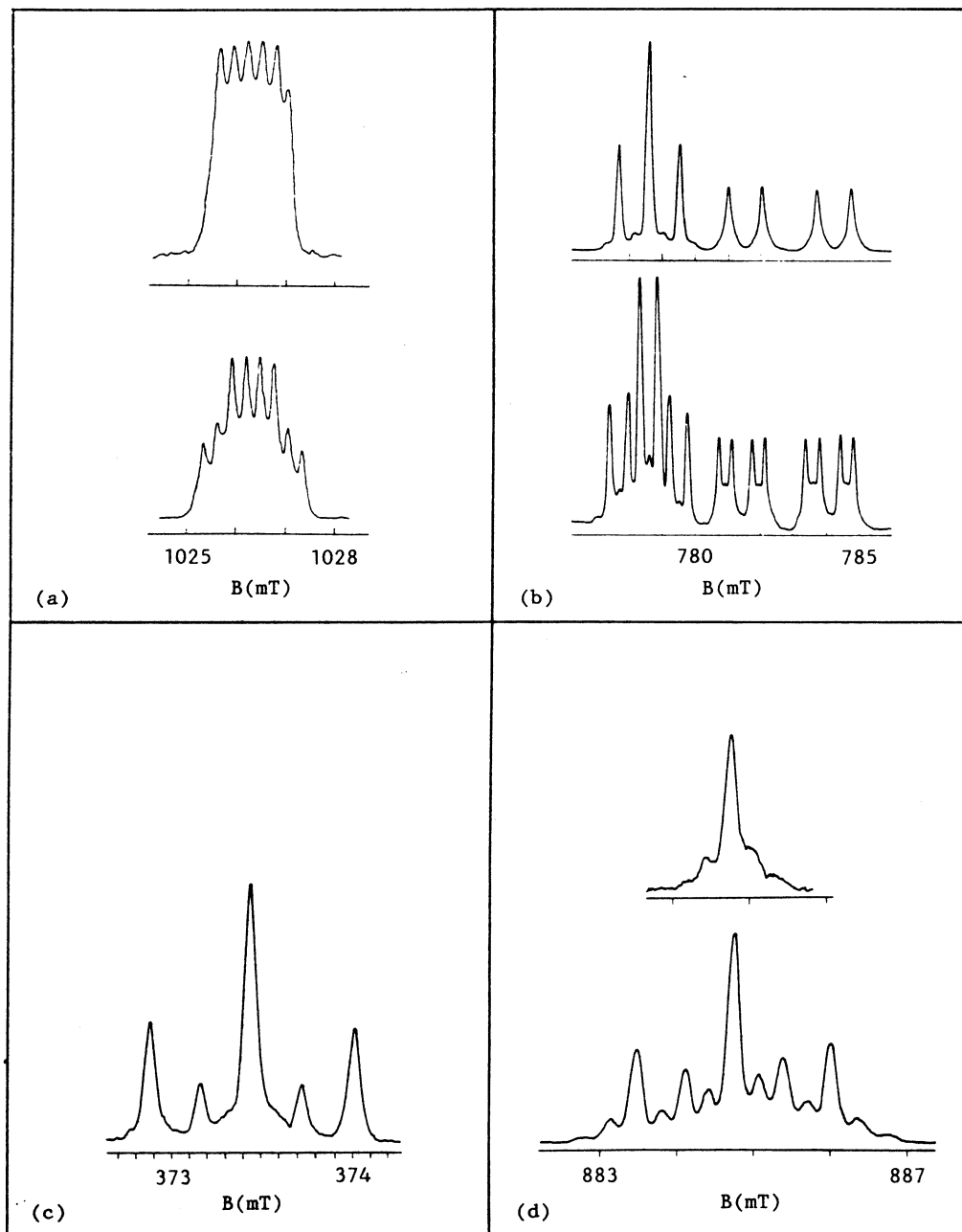


Figure 6. Line shapes of electron paramagnetic resonance spectra showing hyperfine structure due to magnetic impurity nuclei: (a) spectrum NL28 of an FeAl-pair (^{57}Fe , $I=1/2$, 2 and 90%; ^{27}Al , $I=5/2$, 100%), (b) spectrum A23 of the AuFe-pair (^{57}Fe , $I=1/2$, 2 and 90%; ^{197}Au , $I=3/2$, 100%), (c) spectrum NL21 of an $(\text{Fe}_1)_2$ -complex (^{57}Fe , $I=1/2$, 90%), and (d) spectrum NL24 of an $(\text{Fe}_1)_2$ -complex (^{57}Fe , $I=1/2$, 2 and 85%).

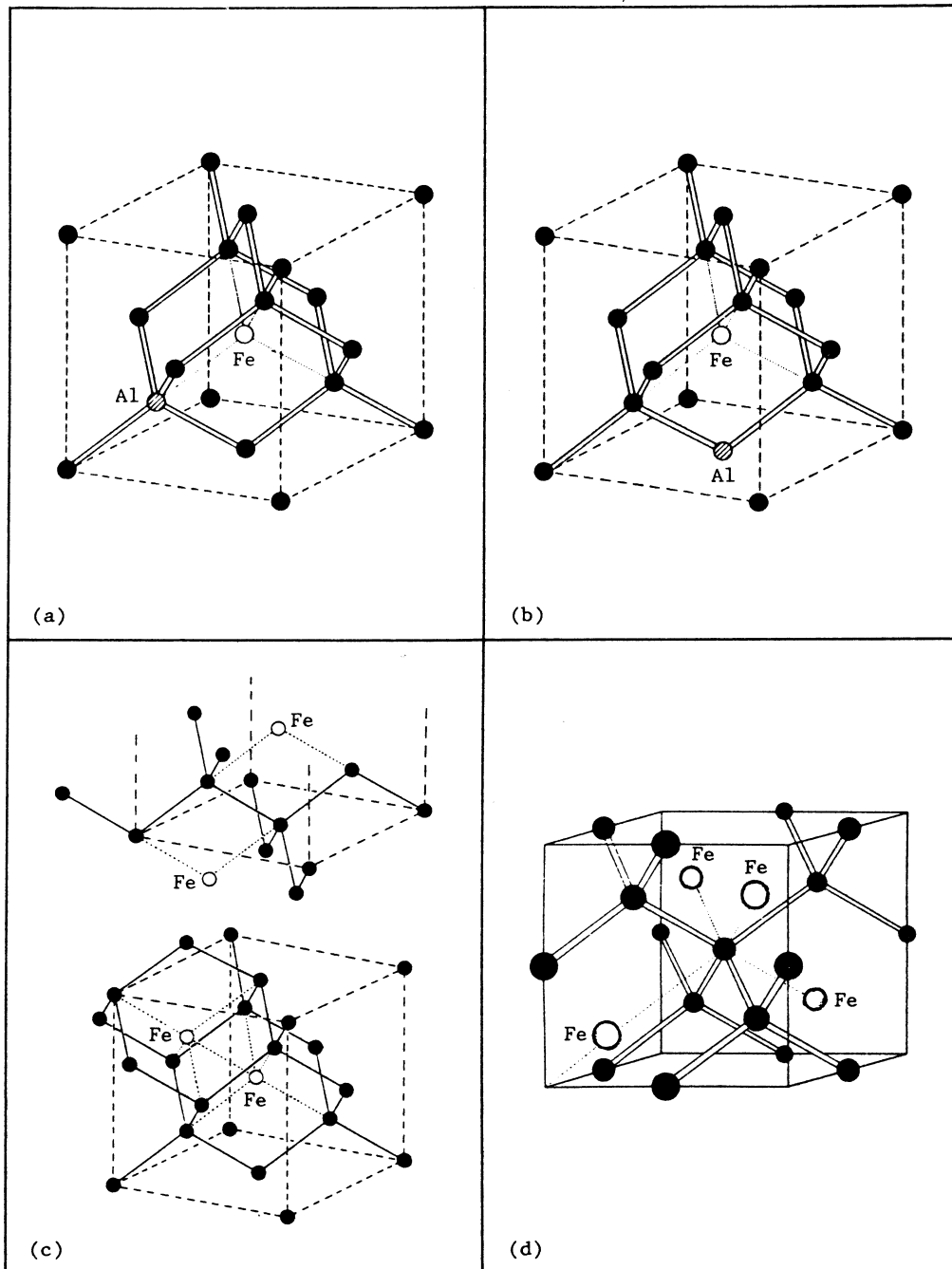


Figure 7. Atomic models for some of the iron-related centres: (a) trigonal FeAl-pair from spectrum NL27, (b) orthorhombic FeAl-pair from spectrum NL28, (c) monoclinic-I FeFe-pair from spectrum NL24, and (d) trigonal $(Fe_i)_4$ -cluster from spectrum NL22.

occupy sites in the silicon crystal. Together these facts derived from the magnetic resonance data put severe constraints on the atomic models for the centres underlying the spectra. Many of the models as given in table I can therefore be considered as quite reliable, some of the models are however more tentative in their detailed structure. Figure 7 provides an illustration of models with varying number of iron atoms or other impurities, and of various symmetries. These pairs and complexes are the initial stages in the process of iron precipitation. For more details of several other properties of the centres, such as their formation kinetics and their anneal, the original literature should be consulted.

REFERENCES

- [1] Graff, K.: Materials Science and Engineering B, to be published
- [2] Ludwig, G.W., Woodbury, H.H., Carlson, R.O.: Phys. Rev. Lett., 1958, 1, 295
- [3] Ludwig, G.W., Woodbury, H.H.: Phys. Rev., 1960, 117, 1286
- [4] Gehlhoff, W., Segsa, K.H.: Phys. Stat. Sol. (b), 1983, 115, 443
- [5] Van Kooten, J.J., Weller, G.A., Ammerlaan, C.A.J.: Phys. Rev. B, 1984, 30, 4564
- [6] Gehlhoff, W., Irscher, K., Kreissl, J.: New Developments in Semiconductor Physics (Springer Verlag, Berlin, 1988), p. 262
- [7] Ludwig, G.W., Woodbury, H.H.: Solid State Physics, Vol. 13 (Academic Press, New York, 1962), p. 223
- [8] Ludwig, G.W.: Phys. Rev., 1965, 137, A1520
- [9] Schirmer, O.F.: Physica, 1983, 116B, 306
- [10] Van Oosten, A.B., Son, N.T., Vlasenko, L.S., Ammerlaan, C.A.J.: Materials Science Forum, 1989, 38-41, 355
- [11] Kleinhenz, R.L., Lee, Y.H., Corbett, J.W., Sieverts, E.G., Muller, S.H., Ammerlaan, C.A.J.: Phys. Stat. Sol. (b), 1981, 108, 363
- [12] Corbett, J.W.: private communication, 1983
- [13] Muller, S.H., Tuynman, G.M., Sieverts, E.G., Ammerlaan, C.A.J.: Phys. Rev. B, 1982, 25, 25
- [14] Van Kooten, J.J., Sieverts, E.G., Ammerlaan, C.A.J.: Solid State Commun., 1987, 64, 1489
- [15] Gehlhoff, W., Irscher, K., Rehse, U.: Materials Science Forum, 1989, 38-41, 373
- [16] Ezhevskii, A.A.: private communication, 1986